

ARTICLE

Received 21 May 2014 | Accepted 23 Jan 2015 | Published 16 Mar 2015

DOI: 10.1038/ncomms7379

IRF8 directs stress-induced autophagy in macrophages and promotes clearance of *Listeria monocytogenes*

Monica Gupta¹, Dong-Mi Shin^{2,3}, Lakshmi Ramakrishna¹, Dennis J. Goussetis⁴, Leonidas C. Platanias^{4,5}, Huabao Xiong⁶, Herbert C. Morse III² & Keiko Ozato¹

Autophagy, activated by many stresses, plays a critical role in innate immune responses. Here we show that interferon regulatory factor 8 (IRF8) is required for the expression of autophagy-related genes in dendritic cells. Furthermore in macrophages, IRF8 is induced by multiple autophagy-inducing stresses, including IFN γ and Toll-like receptor stimulation, bacterial infection, starvation and by macrophage colony-stimulating factor. IRF8 directly activates many genes involved in various steps of autophagy, promoting autophagosome formation and lysosomal fusion. Consequently, *Irf8*^{-/-} macrophages are deficient in autophagic activity, and excessively accumulate SQSTM1 and ubiquitin-bound proteins. We show that clearance of *Listeria monocytogenes* in macrophages requires IRF8-dependent activation of autophagy genes and subsequent autophagic capturing and degradation of *Listeria* antigens. These processes are defective in *Irf8*^{-/-} macrophages where uninhibited bacterial growth ensues. Together these data suggest that IRF8 is a major autophagy regulator in macrophages, essential for macrophage maturation, survival and innate immune responses.

¹Program in Genomics of Differentiation, NICHD, National Institutes of Health, Bethesda, Maryland 20892, USA. ²Laboratory of Immunopathology, NIAID, National Institutes of Health, 5640 Fishers Lane, Room 1421, Rockville, Maryland 20852, USA. ³Department of Food and Nutrition, Seoul National University, Seoul 151-742, Korea. ⁴Robert H. Lurie Comprehensive Cancer Center of Northwestern University, Chicago, Illinois 60611, USA. ⁵Division of Hematology-Oncology, Jesse Brown VA Medical Center, Chicago, Illinois 60612, USA. ⁶Immunology Institute, Mount Sinai School of Medicine, New York, New York 10029, USA. Correspondence and requests for materials should be addressed to K.O. (email: ozatok@nih.gov).

Autophagy is a catabolic process by which misfolded self-proteins and damaged organelles are captured and enzymatically degraded^{1,2}. Autophagy is activated by a variety of stress signals such as starvation and inflammation¹. In macrophages (MΦs) and dendritic cells (DCs), autophagy is also triggered by inflammatory cytokines such as interferon γ (IFN γ), ligands for Toll-like receptors (TLRs) and other pathogen recognition receptors and is required for innate clearance of invading pathogens^{3–6}. The absence of autophagy genes such as *Atg5* and *Atg7* impairs pathogen recognition activity, type I IFN production and increases susceptibility to pathogens, including *Mycobacterium (M) tuberculosis* and *Listeria monocytogenes*^{7–10}. Recent studies indicate that autophagy is involved in M-CSF-induced differentiation of monocytes to MΦs^{11,12}.

Autophagy follows a well-ordered sequence of events where the activation of ULK1 and Beclin1 leads to LC3 lipidation and autophagosome formation. Autophagosomes then fuse with lysosomes to allow the hydrolysis of captured materials. Autophagic degradation is linked to the ubiquitin conjugation pathway, as some ubiquitinated proteins are escorted to autolysosomes through ubiquitin adaptors such as SQSTM1 (p62) to allow proteasome independent degradation^{10,13,14}. IFN γ -induced GTPases, such as IRGM1, are recruited to the autolysosomes and facilitate autophagic clearance of bacteria¹⁵.

It is thought that autophagic activation and the subsequent elimination of captured molecules are directed by a mechanism that unifies and coordinates complex autophagic processes¹. Although our understanding on this aspect of autophagy is limited, there are a few examples where autophagic events are joined together as a defined network: in these cases, transcription factors, such as TEFB and FOXO3 act as autophagy master regulators in a cell type- and signal-dependent manner^{16,17}.

Interferon regulatory factor 8 (IRF8) is a transcription factor that promotes the differentiation of MΦs and DC subsets^{18,19}. IRF8 is induced by IFN γ plus TLRs in MΦs and stimulates genes important for host defense, including type I IFNs, promoting the production of reactive oxygen species and nitric oxide^{20,21}. IRF8 is essential for innate resistance against intracellular bacteria, including *M. tuberculosis*, *M. Bovis (BCG)*, *Salmonella* and *Listeria*, although underlying mechanisms have not been fully understood^{22–26}.

We show here that IRF8 is induced in MΦs and DCs by diverse stresses that activate autophagy and stimulates transcription of many autophagy genes, thereby facilitating the entire autophagic processes. Accordingly, *Irf8*^{−/−} MΦs are defective in various steps of autophagy induced by IFN γ /TLR stimulation, *Listeria* infection, starvation and macrophage colony-stimulating factor (M-CSF). As a result, ubiquitin-linked SQSTM1 accumulates in greater amounts in *Irf8*^{−/−} MΦs than wild-type (WT) MΦs. Further, infection by *Listeria monocytogenes* leads to a dramatically induced IRF8 that coincides with marked activation of multiple autophagy genes, which results in autophagic control of bacterial growth. *Irf8*^{−/−} MΦs are, however, unable to activate autophagy genes and succumb to uninhibited *Listeria* growth. Transfer of the *Irf8* gene into *Irf8*^{−/−} MΦs partially rescues the expression of autophagy genes and autophagic activity in *Listeria* infected MΦs. Together, IRF8 is an autophagy master regulator that acts in MΦs to meet diverse stresses.

Results

Microarray analyses reveal a role of IRF8 in autophagy. Previous genome-wide studies reported that IRF8 regulates more than 1,500 genes in monocytes, MΦs and B cells^{21,27,28}. To gain genome-wide information on IRF8 in DCs, we performed microarray analyses with bone marrow (BM)-derived DCs from

WT and *Irf8*^{−/−} mice on stimulation by TLR ligands, lipopolysaccharide (LPS) and CpG. With a cutoff line of $>2 \times$ with $P \leq 0.05$ (identified by one-way analysis of variance), 326 and 713 genes were expressed higher in WT DCs than in *Irf8*^{−/−} DCs in untreated (UT) and TLR-stimulated DCs, respectively (Fig. 1a, left), whereas the expressions of 350 and 648 genes were lower in WT DCs than in *Irf8*^{−/−} DCs (Fig. 1a, right). Thus, IRF8 regulates many constitutive and TLR-stimulated genes in DCs either positively or negatively, as reported before for other cell types^{21,27,28}. Gene ontology (GO) analysis of positively regulated genes showed significant enrichment for immune system processes, inflammatory responses, lysosome functions, while genes negatively regulated by IRF8 were enriched with cell cycle, cell division and DNA replication (Supplementary Fig. 1a,b). A large number of TLR-stimulated genes were upregulated by IRF8, consistent with previous reports that IRF8 is critical for TLR activation of DCs (Supplementary Fig. 1c and Supplementary Table 1)^{18,20,29}. Eleven percent of those were found in the Interferome, confirming a functional link between IRF8- and IFN-related regulation (<http://interferome.org/>)³⁰ (Supplementary Fig. 1d).

Inspection of IRF8-stimulated genes belonging to the category of immune system processes and lysosome functions (Supplementary Fig. 1a) revealed that a number of genes in the autophagy pathway are downregulated in *Irf8*^{−/−} DCs (Fig. 1b and Supplementary Table 2). These genes, except for *Atg2a*, were induced after TLR, as confirmed by quantitative reverse transcription-PCR (qRT-PCR) analysis (Fig. 1c). Because IRF8 regulates shared sets of genes in DCs and MΦs and autophagy has been extensively investigated in MΦs, we hereafter studied the role of IRF8 in MΦ autophagy. The expressions of 24 autophagy genes were first tested in BM-derived MΦs from WT and *Irf8*^{−/−} mice stimulated with IFN γ overnight followed by TLR ligands, LPS and CpG: IFN γ and TLR ligands provide priming and triggering signals, respectively, which together boost autophagic activity in MΦs^{31,32}. Data in Fig. 1d showed that 17 autophagy genes were downregulated in *Irf8*^{−/−} MΦs relative to WT MΦs and that all but *Atg7* were induced by IFN γ plus TLR (IFN γ /TLR) stimulation. *Atg7* expression, which fell after stimulation, was also consistently lower in *Irf8*^{−/−} MΦs than WT cells. These genes represent essentially all phases of autophagy (see Fig. 1d, left). As reported previously, IFN γ /TLR treatment also stimulated *Irf8* expression^{18,19}. The remaining seven genes were not induced by IFN γ /TLR and did not differ in WT and *Irf8*^{−/−} MΦs (Supplementary Fig. 2). These results indicate that many autophagy genes are induced by IFN γ /TLR stimulation in an IRF8-dependent manner.

Rescue experiments in Fig. 1e showed that transfer of the *Irf8* gene into *Irf8*^{−/−} MΦs restored the expression of 10 autophagy genes on IFN γ /TLR stimulation. As expected, *Irf8* transfer did not restore the expressions of these genes in unstimulated MΦs. The transcriptionally defective mutant, *Irf8K79E*, in contrast, failed to rescue these autophagy genes. It is of note that *Irf8* transfer did not rescue all 17 genes, which may be attributed to insufficient levels of IRF8 expression, insufficient post-translational changes in IRF8 proteins or other mechanisms.

IRF8 binds to and stimulates autophagy genes in MΦs. Seven of the 17 autophagy genes upregulated by IRF8 carried IRF8-binding motifs within the 3.5-kb upstream promoter region (Fig. 2a)^{19,33}. We performed qPCR-based chromatin immunoprecipitation (ChIP) analysis to test the binding of IRF8 to these genes in MΦs. As shown in Fig. 2b, IRF8 bound to all seven genes in WT MΦ, but not in *Irf8*^{−/−} MΦs. IRF8 binding increased after IFN γ /TLR stimulation for most of the genes,

consistent with enhanced mRNA expression after stimulation (Fig. 1d). Consistent with the expression data, *Atg7* showed high IRF8 binding in UT WT MΦs, and the expression fell slightly after stimulation. Figure 2c summarizes the data for mRNA expression, rescue by IRF8 and ChIP assay, illustrating that IRF8 stimulates transcription of many autophagy genes constitutively and after IFNγ/TLR stimulation.

***Irf8*^{-/-} MΦs are defective in IFNγ/TLR-induced autophagy.** To test whether defective gene expression in *Irf8*^{-/-} MΦs affects autophagic functions, we next examined the autophagosome formation in MΦs expressing mCherry-enhanced green

fluorescent protein (EGFP)-LC3B (Fig. 3a). This vector detects acid-sensitive (EGFP) and -resistant (mCherry) LC3, enabling us to assess the formation of autophagosomes and the subsequent fusion with lysosomes³⁴. Before stimulation, GFP and mCherry signals were diffusely distributed over the cytoplasm both in WT and *Irf8*^{-/-} MΦs. After IFNγ/TLR stimulation, GFP and mCherry signals relocated to form prominent punctate structures representing autophagosomal vesicles in WT cells (see arrows in Fig. 3a). In contrast, few fluorescent vesicles were seen in *Irf8*^{-/-} MΦs. Quantification in Fig. 3a (lower panel) confirmed that the number of cells with fluorescent vesicles was much fewer in *Irf8*^{-/-} MΦs. Deficiency in *Irf8*^{-/-} MΦs to

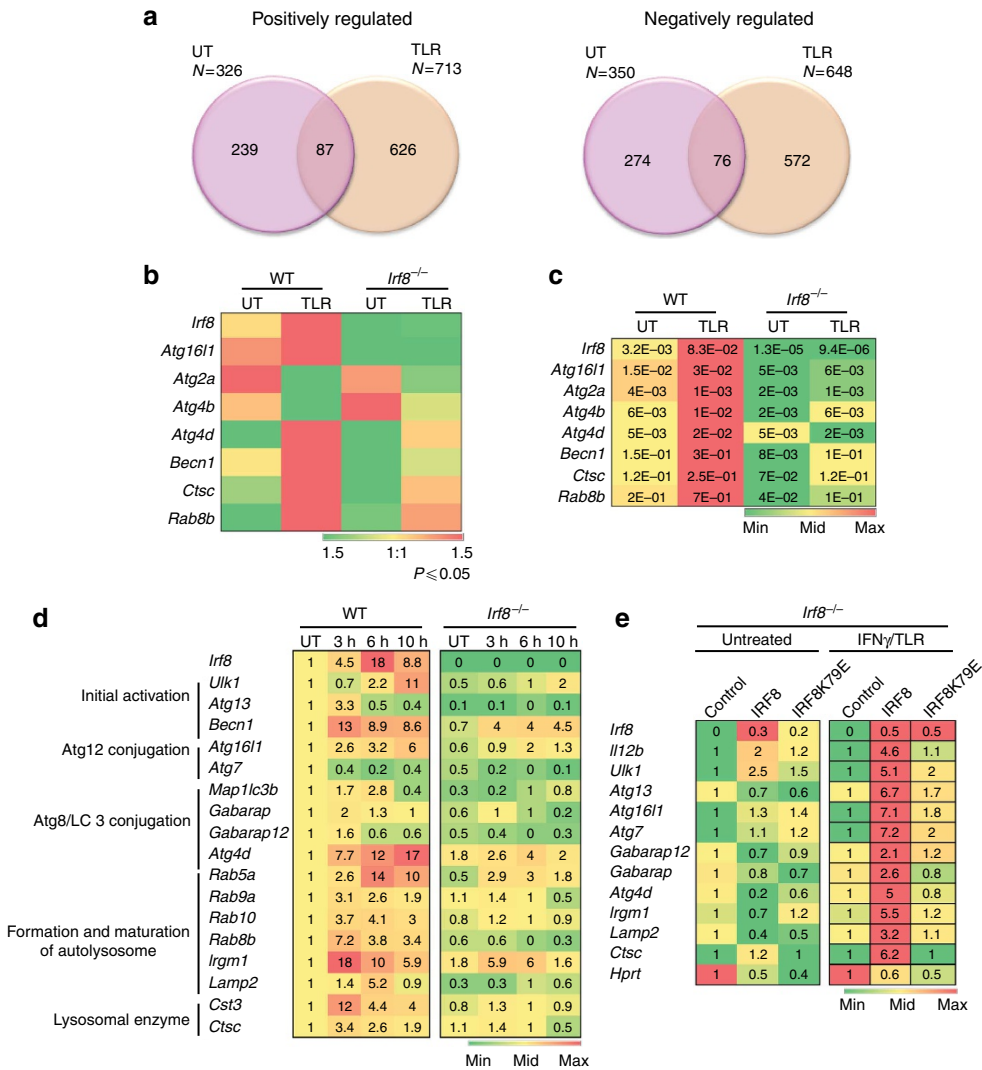


Figure 1 | Microarray analyses reveal a role of IRF8 in autophagy. (a) The Venn diagrams depict the number of genes positively and negatively regulated by IRF8 in UT DCs and those treated with TLR ligands for 6 h identified by microarray analysis. Overlapped regions represent the number of genes positively or negatively regulated both in UT and TLR-stimulated DCs. See GO classification in Supplementary Fig. 1a,b. (b) IRF8-dependent autophagy genes identified by microarray analysis. Differentially expressed genes were identified by one-way analysis of variance ($P \leq 0.05$ and fold change ≥ 2). Colour gradients indicate average signal intensities of genes in log2 scale. Normalization was performed by GeneChip Operating Software (GCOS) and Expression Console software's relative to the UT. (c) qRT-PCR analysis of IRF8-dependent autophagy genes in DCs. WT and *Irf8*^{-/-} DCs were stimulated with the TLR ligands for 6 h. The numbers represent transcript levels normalized by *gapdh* levels. Data represent the average of three independent assays. $P \leq 0.01$, Student's *t*-test. (d) qRT-PCR analysis of IRF8-dependent autophagy genes in MΦs. WT and *Irf8*^{-/-} MΦs were treated overnight with IFNγ and stimulated with TLR ligands for the indicated times. The number in each box represents transcript levels normalized by the value of UT WT cells. Values are the average of three independent assays. $P \leq 0.01$ (Student's *t*-test). See autophagy genes not affected by IRF8 in Supplementary Fig. 2. (e) *Irf8*^{-/-} MΦs were transduced with pMSCV retroviral vector containing WT *Irf8* or mutant *Irf8* (K79E), and stimulated with IFNγ/TLR for 8 h. Relative expression of indicated autophagy genes was detected by qRT-PCR. The numbers represent transcript levels normalized by those of cells transduced with empty vector. *Irf8* expression was normalized by *gapdh*. Values are the average of three experiments. $P \leq 0.05$ (Student's *t*-test). *Il12b* and *Hprt* were tested as controls.

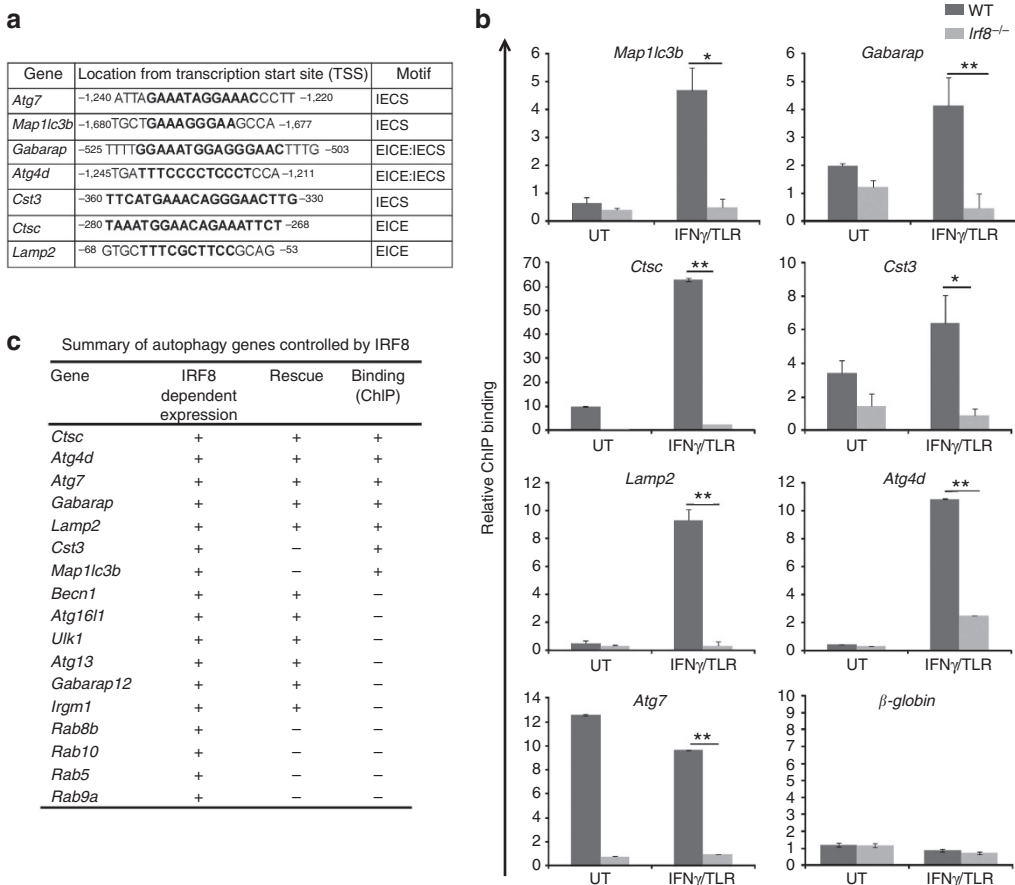


Figure 2 | IRF8 binds to the promoters of autophagy genes. (a) Consensus IRF8-binding motifs are shown in bold on indicated autophagy gene promoters. (b) IRF8 binding to the above motifs was detected by ChIP for WT and *Irf8*^{-/-} MΦs (UT or treated with IFN γ /TLR) normalized by normal IgG binding, and with β -globin as a negative control. Values represent the average of five independent experiments. **P* ≤ 0.05 and ***P* ≤ 0.01. (Student's *t*-test). (c) Summary of qRT-PCR analysis rescue experiment and ChIP assays.

form LC3 vesicles was also evident with endogenous LC3 (Supplementary Fig. 3a). Electron microscopy analysis additionally showed a noticeable increase in autophagic vesicles in stimulated WT MΦs, but not in *Irf8*^{-/-} MΦs (Fig. 3b, right panel)³⁵. Immunoblot analysis was performed to assess phosphatidylethanolamine conjugation of LC3 as detected by changes in LC3I and LC3II levels³⁶. Cells were treated with bafilomycin A1 to block the fusion of autophagosomes to lysosomes³⁶. Data in Fig. 3c (right panel) showed the amounts of LC3II increased in WT MΦs after IFN γ /TLR stimulation. LC3II levels were significantly lower in *Irf8*^{-/-} MΦs before stimulation and did not measurably increase after stimulation, as confirmed by quantification (Fig. 3c, right panel). Flow cytometric analysis to detect membrane-bound LC3 further validate these results, in that LC3 signals increased after stimulation in WT MΦs. However, LC3 levels were lower in *Irf8*^{-/-} MΦs before stimulation and remained low after stimulation (Fig. 3d)³⁷. To ascertain whether IRF8 has a role in autophagosome-lysosome fusion and lysosomal clearance, immunoblot and flow cytometry assays were performed in the absence of bafilomycin A1 (Supplementary Fig. 3b,c)³⁶. In WT MΦs, the amounts of LC3 hardly increased after stimulation, suggesting lysosomal turnover of LC3. On the other hand, LC3 levels were again lower in *Irf8*^{-/-} MΦs and the amounts were unchanged after stimulation. These data support the notion that IRF8 plays a role in autophagosome formation, and subsequent autophagolysosome formation and function in IFN γ /TLR-induced autophagy. Further supporting the role of IRF8 in

autophagosome formation, the amounts of Atg5-Atg12 complex increased in WT MΦs, but not in *Irf8*^{-/-} MΦs on IFN γ /TLR stimulation (Fig. 3e). We noted that although autophagy is linked to the down-regulation of mammalian target of rapamycin (mTOR) kinase in a starvation model¹, IFN γ /TLR stimulation did not downregulate phospho-mTOR expression, but it rather upregulated it in WT and *Irf8*^{-/-} MΦs (Supplementary Fig. 4), indicating that IFN γ /TLR-induced autophagy may not be directly controlled by mTOR activity, consistent with the recent report⁵. As autophagy proceeds further, autophagosomes fuse with lysosomes to become autolysosomes that carry LC3 and various lysosome-associated components². LAMP2, a lysosomal membrane protein, is involved in the autophagosome-lysosome fusion³⁸. Immunostaining and immunoblot data in Fig. 4a,b found that LAMP2 expression was lower in *Irf8*^{-/-} MΦs than in the WT cells, consistent with reduced *Lamp2* mRNA expression in *Irf8*^{-/-} cells (Fig. 1d). To test whether IRF8 affects autolysosome formation, we examined the co-localization of endogenous LC3 and lysosomes as detected by LysoTracker-red by immunostaining³⁶. Immunostaining data in Fig. 4c showed that the majority of LC3 vesicles merged with LysoTracker-red staining in WT MΦs on IFN γ /TLR stimulation (arrow heads). However, in *Irf8*^{-/-} MΦs, LC3 and LysoTracker-red double positive vesicles were much fewer (Fig. 4c). These results indicate that through transcriptional control, IRF8 indirectly facilitates maturation of autophagosomes to autolysosomes in response to IFN γ /TLR stimulation.

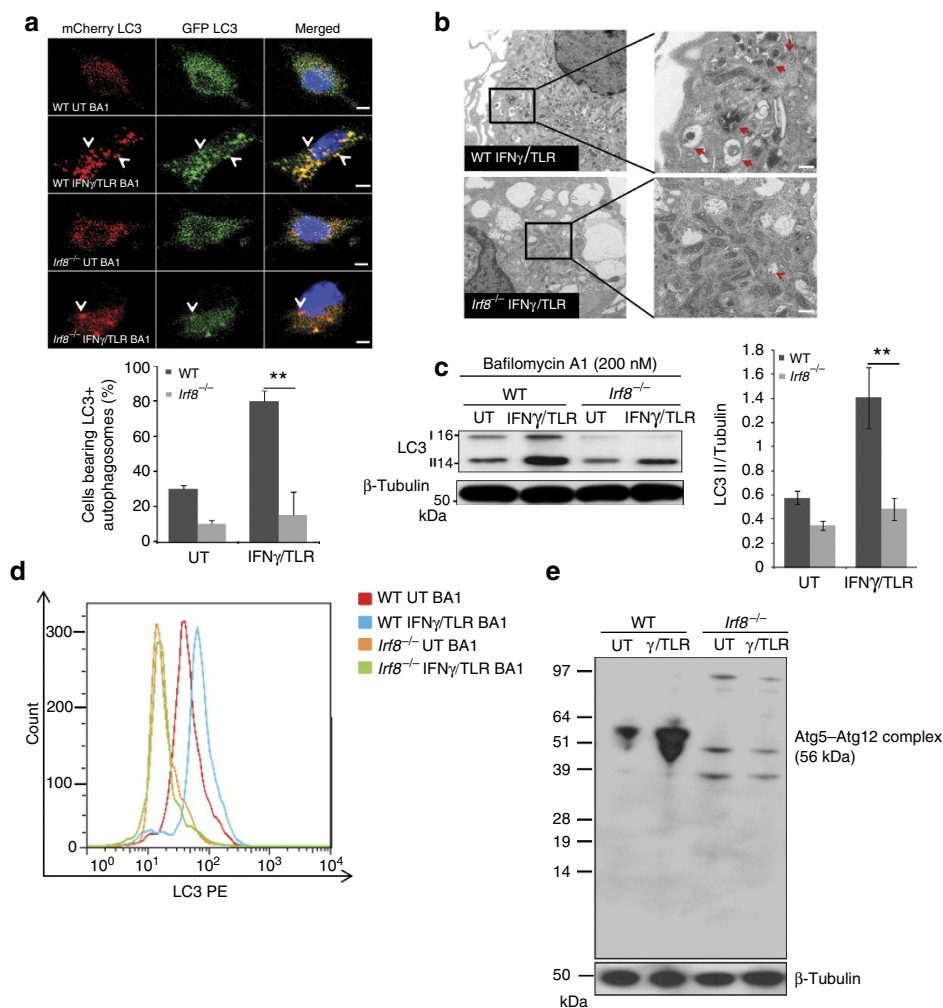


Figure 3 | Defective autophagosome formation in *Irf8*^{-/-} MΦs. (a) LC3 vesicles were visualized in WT and *Irf8*^{-/-} MΦs expressing mCherry-EGFP-LC3 vector, without (UT) or with IFN γ /TLR stimulation for 8 h. Bafilomycin A1 (BA1; 200 nM) was added for the final 2 h. Cells were counterstained for DNA (blue). Scale bar, 20 μ m. Below: the number of cells with more than five mCherry-positive vesicles was counted by microscopic inspection of more than 200 cells. The values represent the percentage of cells with fluorescent vesicles. $^{**}P \leq 0.01$ (Student's *t*-test). See Supplementary Fig. 3a for endogenous staining of LC3. (b) WT and *Irf8*^{-/-} MΦs treated with IFN γ overnight followed by TLR ligands for 8 h was inspected by transmission electron microscopy. The bracketed region in the left panel was enlarged in the right panel. Arrows indicate autophagic vacuoles. Scale bar, 0.5 μ m. (c) Reduced LC3I to LC3II conversion in *Irf8*^{-/-} MΦs. WT and *Irf8*^{-/-} MΦs were treated with IFN γ /TLR as above with BA1 (200 nM) treatment for the final 2 h. Immunoblot analysis was performed with 10 μ g of extracts with β -Tubulin as a control. Right panel: the amounts of LC3II in three independent samples were quantified using the ImageJ software. $^{*}P \leq 0.05$ and $^{**}P \leq 0.01$ (Student's *t*-test). See Supplementary Fig. 3b for LC3 amount in the absence of BA1. (d) Membrane-bound LC3 in WT and *Irf8*^{-/-} MΦs treated with IFN γ /TLR was detected by flow cytometry. BA1 (200 nM) was added for the final 2 h. The histogram is a representative of three independent experiments. See Supplementary Fig. 3c for LC3 amount in the absence of BA1. (e) Immunoblot detection of the ATG5-ATG12 conjugate. WT and *Irf8*^{-/-} MΦs were treated as above and immunoblot detection of the ATG5-ATG12 conjugate proteins was performed. Ten micrograms of the extracts were tested with antibody against ATG5 or β -Tubulin.

***Irf8*^{-/-} MΦs accumulate SQSTM1/ubiquitinated proteins.** Misfolded self-proteins and invading pathogens are often conjugated to ubiquitin and escorted to autophagosomes to be degraded in lysosomes. This process is partly mediated by the ubiquitin adaptor SQSTM1 (p62)^{13,14}. Some autophagy-deficient cells form aggregates, called aggresomes or inclusion bodies that contain SQSTM1 and ubiquitin¹⁴. In light of defective autophagy, it was possible that *Irf8*^{-/-} MΦs abnormally accumulate SQSTM1 and ubiquitin-containing proteins. Immunostaining of ubiquitin and SQSTM1 showed extensive deposition of SQSTM1 that co-localized with ubiquitin-positive proteins in *Irf8*^{-/-} MΦs after IFN γ /TLR stimulation, in contrast to WT MΦs that showed little deposition of these proteins (Fig. 5a, left panel). Quantification of SQSTM1 and ubiquitin-positive cells confirmed

the immunostaining results (Fig. 5a, right panel). Immunoblot analysis further confirmed that SQSTM1 accumulates in greater amounts in *Irf8*^{-/-} than WT MΦs with and without bafilomycin A1 treatment (Fig. 5b upper panel and Supplementary Fig. 3b). In addition, the amounts of ubiquitin-positive proteins increased markedly after stimulation and to a greater extent in *Irf8*^{-/-} MΦs than WT cells (Fig. 5b, left and right panels). In agreement with the increased ubiquitin-positive proteins, we previously noted that IFN γ /TLR stimulation increases ubiquitin-conjugated proteins in MΦs³⁹. Next, we tested whether the larger increase in SQSTM1 protein expression in *Irf8*^{-/-} cells was due to higher *Sqstm1* transcription in *Irf8*^{-/-} MΦs. Relevant to this question, we previously showed that *Sqstm1* mRNA expression increases after IFN γ /TLR stimulation

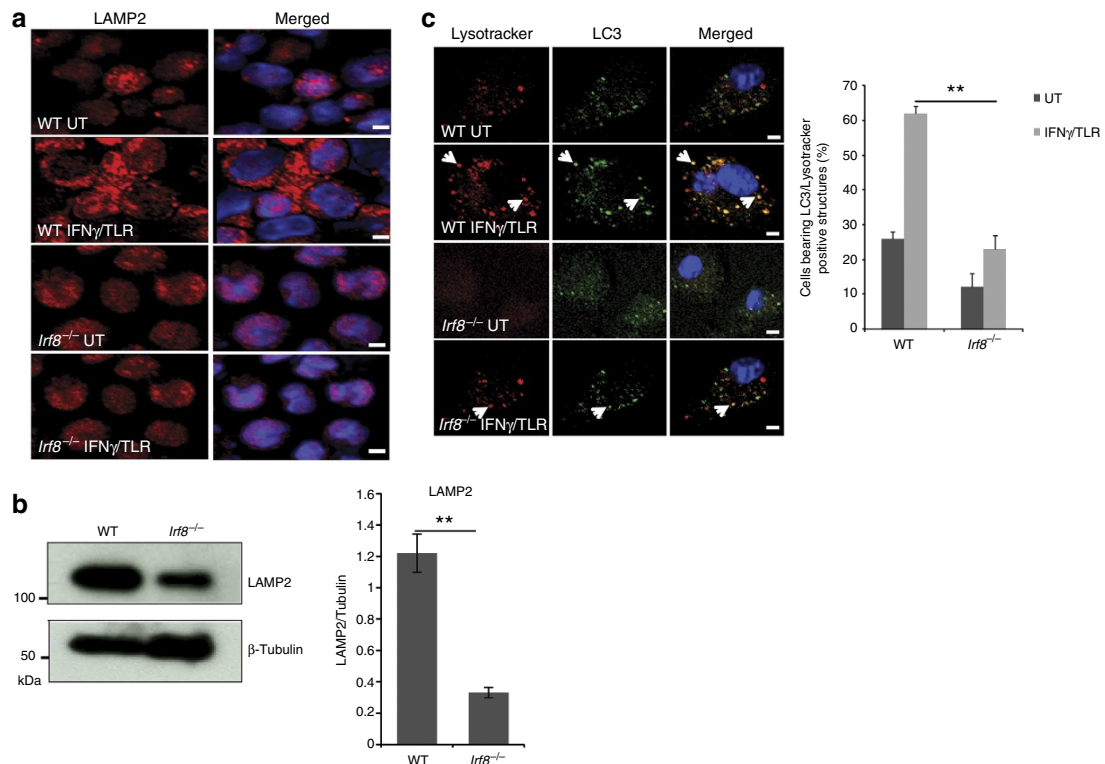


Figure 4 | Defective autophagosome maturation in *Irf8*^{-/-} MΦs. (a) Immunostaining of LAMP2 in WT and *Irf8*^{-/-} MΦs stimulated with IFN γ overnight and TLR ligands for 8 h. Cells were counterstained for DNA (blue). Scale bar, 20 μ m. (b) Immunoblot detection of LAMP2 in WT and *Irf8*^{-/-} MΦs. Ten micrograms of extracts were tested with antibody against LAMP2 or β -Tubulin. Below: the amounts of LAMP2 in three independent experiments were quantified using the ImageJ software. ** $P \leq 0.01$. (c) WT and *Irf8*^{-/-} MΦs were immunostained for LC3 antibody and LysoTracker-red to detect LC3-positive and lysosome-positive structures. Right: cells with double-positive vesicles were quantified as in Fig. 3a. Data represent the average of three independent experiments. $P \leq 0.01$ (**). Scale bar, 20 μ m.

in WT MΦs⁴⁰. qRT-PCR data showed that the levels of *Sqstm1* mRNA were comparable in WT and *Irf8*^{-/-} MΦs, indicating that SQSTM1 proteins aberrantly accumulate in *Irf8*^{-/-} cells after stimulation, due to deficiency in autophagic degradation (Supplementary Fig. 5). To ascertain the role of autophagic degradation in the elimination of ubiquitin-conjugated proteins, in addition to proteasome mediated degradation, immunoblot analysis was performed for cells treated with a proteasome inhibitor, MG132. As seen in Fig. 5c left and right panels, *Irf8*^{-/-} MΦs accumulated greater amounts of ubiquitin-bound proteins than WT MΦs in the presence of MG132, suggesting that autophagy partly accounted for excess accumulation of SQSTM1 and ubiquitin-bound proteins in *Irf8*^{-/-} MΦs. Further supporting the accumulation of unprocessed proteins in *Irf8*^{-/-} MΦs, MitoTracker-positive materials that co-localized with monodansylcadaverine staining were more abundant in *Irf8*^{-/-} MΦs than WT cells (Supplementary Fig. 6)³⁶.

IRF8 is required for autophagic clearance of *Listeria*.

Autophagy is a major mechanism by which MΦs eliminate intracellular bacteria, such as *M. tuberculosis*, *Salmonella* and *Listeria*^{6,10,41}. Previous studies showed that IRF8 is essential for controlling infection of the above bacteria^{22–26}. However, it has not been clear whether IRF8 employs autophagy to confer protection. We first examined whether *Listeria* infection activates autophagy genes in MΦs: *Listeria monocytogenes* is a food-borne pathogen that causes listeriosis and is widely studied in mouse models⁴². qRT-PCR data in Fig. 6a showed that the expression of

Listeria transcripts rose sharply in *Irf8*^{-/-} MΦs during 48 h of infection, while remained very low in WT MΦs, including ActA shown to bypass host cell autophagy⁴¹. On the other hand, *Listeria* infection markedly increased expression of many autophagy genes in WT MΦs, in some cases by nearly 100-folds (Fig. 6b). Among induced genes was *Nod1*, important for autophagy-mediated control of *Listeria*⁴³. Interestingly, on *Listeria* infection, *Irf8* expression was also dramatically increased. In contrast, none of these autophagy genes were induced in *Irf8*^{-/-} MΦs at comparable levels (Fig. 6b). Accordingly, while WT MΦs restricted bacterial growth to a minimum, *Irf8*^{-/-} MΦs relented to the logarithmic growth of *Listeria*, as verified by bacterial accumulation in the cytoplasm (Fig. 6c). Further supporting IRF8-dependent autophagic activation, LC3II levels increased during *Listeria* infection in WT MΦs but not in *Irf8*^{-/-} MΦs, as observed in the presence of bafilomycin A1 (Fig. 6d). In contrast, LC3II amounts remained much lower in *Irf8*^{-/-} MΦs during infection. In the absence of bafilomycin A1, LC3II amounts increased at 24 h, then gradually decreased afterwards up to 48 h (Supplementary Fig. 7a) in WT MΦs. In *Irf8*^{-/-} MΦs, LC3II amounts also increased at 24 h, but remained high throughout 48 h of infection, suggesting inefficient LC3 turnover in lysosomes^{36,44}. In agreement, SQSTM1 and SQSTM1-positive proteins accumulated in *Irf8*^{-/-} MΦs in greater amounts than WT cells with and without bafilomycin A1 (Fig. 6d, Supplementary Fig. 7a). Together these results reinforce the view that during *Listeria* infection, IRF8 plays a major role in promoting both autophagosome formation and the subsequent autolysosomal functions. Importantly, immunostaining analysis in Fig. 6e revealed that *Listeria* antigens co-localized with LC3

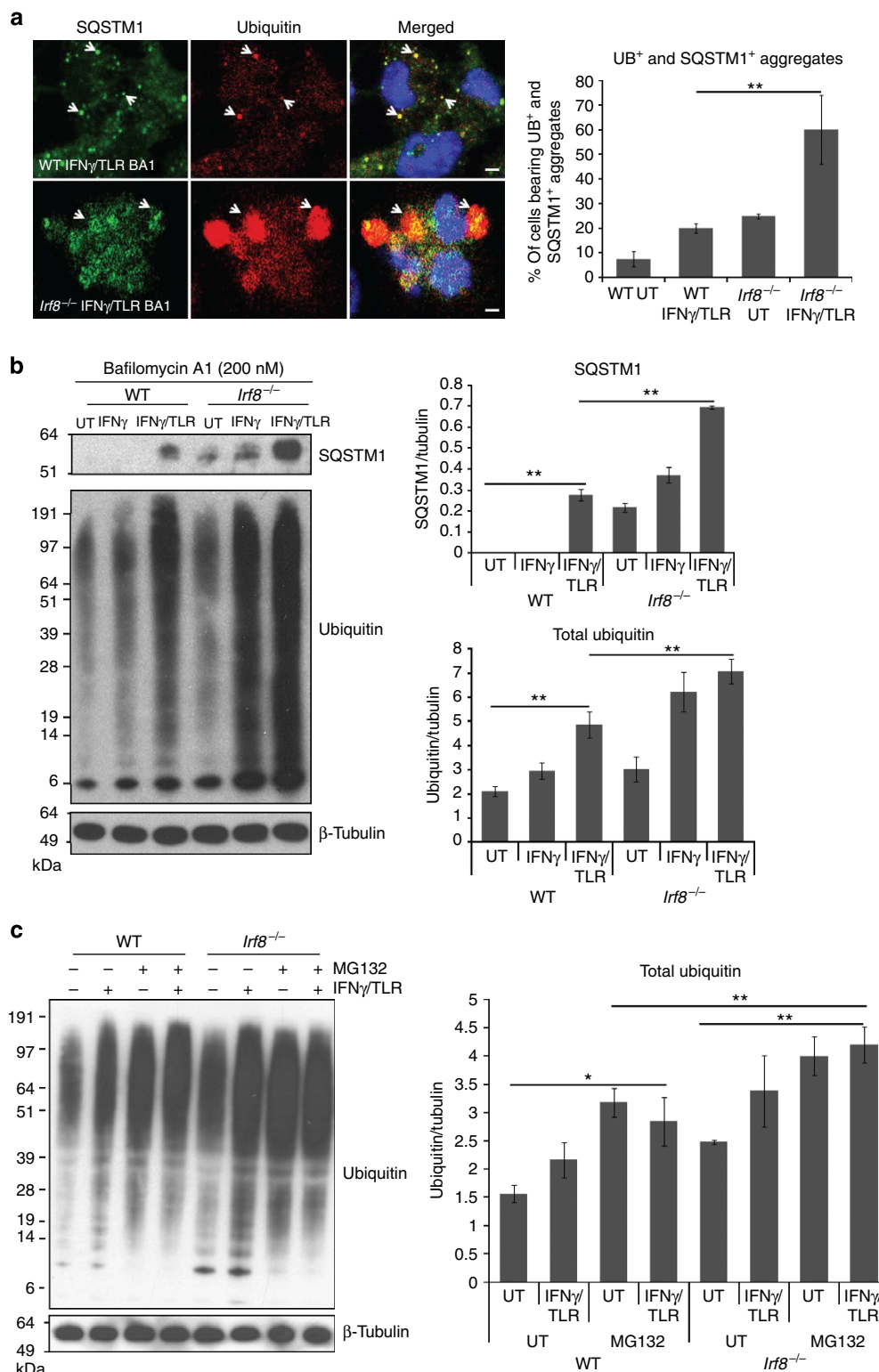
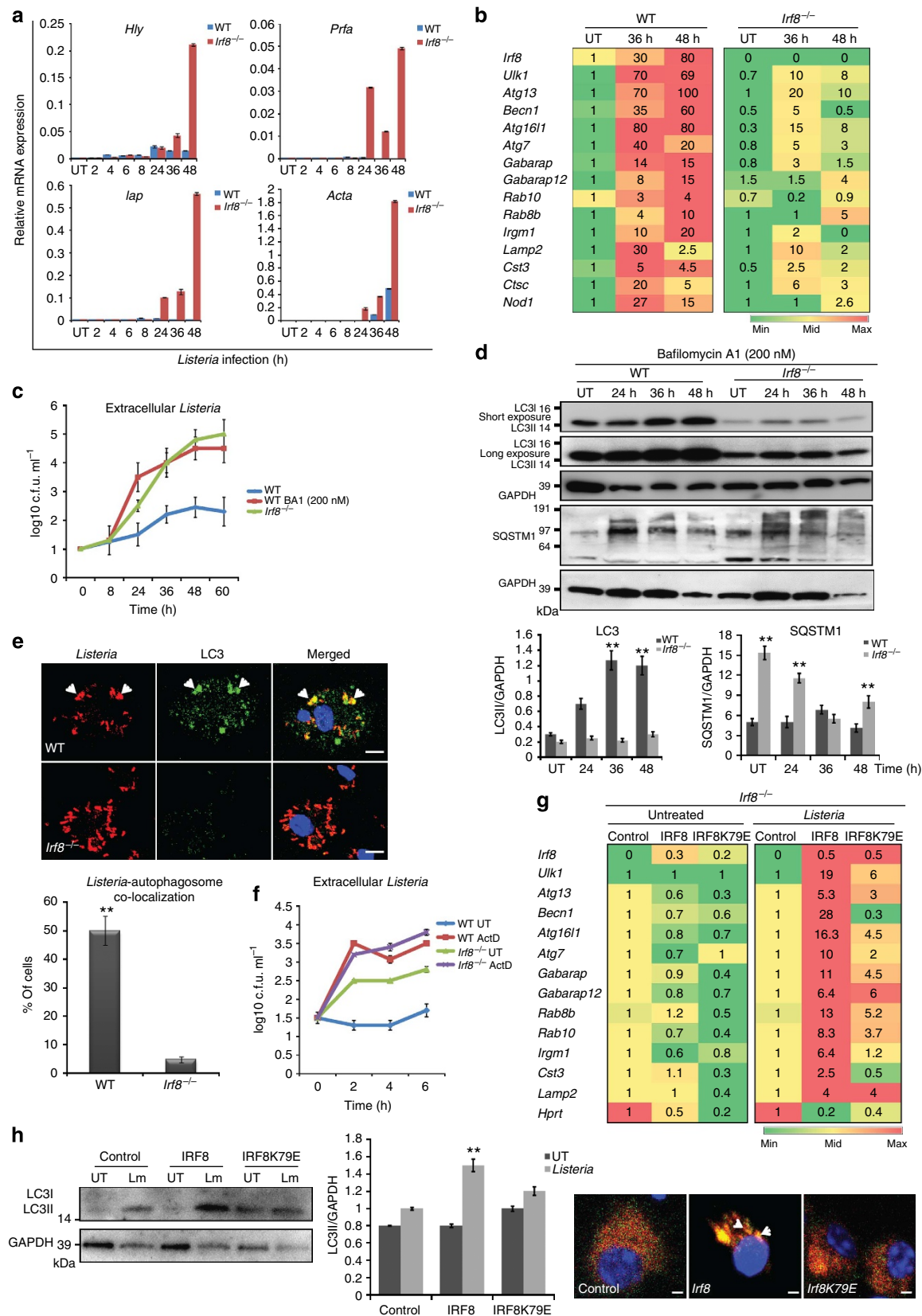


Figure 5 | SQSTM1 and ubiquitin-conjugated proteins form aggregates in *Irf8*^{-/-} MΦs. (a) SQSTM1- and ubiquitin-positive proteins (arrow heads) in WT and *Irf8*^{-/-} MΦs stimulated with IFN γ overnight and TLR ligands for 8 h were visualized by immunostaining. Bafilomycin A1 (200 nM) was added for the final 2 h. Cells were counterstained for DNA (blue). Right panel: the percentage of cells with SQSTM1- and ubiquitin-positive aggregates. Data represent the average of three independent experiments \pm s.d. with $**P \leq 0.01$ (Student's *t*-test). **(b)** Immunoblot detection of SQSTM1- and ubiquitin-positive proteins in WT and *Irf8*^{-/-} MΦs stimulated with IFN γ or IFN γ /TLR for 8 h. Bafilomycin A1 (200 nM) was added for the final 2 h. Right panel: relative amounts of ubiquitin-bound proteins. Data represent the average of three independent experiments \pm s.d. with $**P \leq 0.01$ (Student's *t*-test). See Supplementary Fig. 3b for immunoblot detection of SQSTM1 in the absence of bafilomycin A1. **(c)** Immunoblot detection of ubiquitin-bound proteins in the presence of MG132. WT and *Irf8*^{-/-} MΦs were stimulated with IFN γ /TLR in the presence of 10 μ M of MG132. Right panel: relative amounts of ubiquitin-bound proteins. Data represent the average of three independent experiments \pm s.d. with $*P \leq 0.05$ and $**P \leq 0.01$ (Student's *t*-test).

and formed autophagosomal vesicles in WT cells, indicative of autophagic capturing of bacterial antigens. However, the *Listeria* antigens were more abundant in *Irf8*^{-/-} MΦs than in WT cells and the co-localization with LC3 was hardly observed (Fig. 6e). We also found that blocking of autophagosome-lysosome fusion

by bafilomycin A1 led to logarithmic growth of *Listeria* in WT MΦs, comparable to that in *Irf8*^{-/-} MΦs, supporting autophagic control of *Listeria* infection (Fig. 6c). To ascertain whether autophagic control of *Listeria* relies on *de novo* transcription of autophagy genes, infected WT and *Irf8*^{-/-}



MΦs were briefly treated with Actinomycin D (Act D) and tested for bacterial growth. As shown in Fig. 6f, bacterial counts sharply increased after 2 h of Act D treatment both in WT and *Irf8*^{-/-} MΦs. Act D also inhibited autophagosome formation and expression of autophagy genes on IFNγ/TLR stimulation (Supplementary Fig. 8). These results are analogous to the previous report where muscle cell autophagy depends on FOXO3-mediated transcription of autophagy genes¹⁷.

Rescue experiments in Fig. 6g showed that transfer of the WT *Irf8* gene into *Irf8*^{-/-} MΦs restored expression of most of the autophagy genes induced by *Listeria* shown in Fig. 6b. In contrast, none of these genes were rescued by the mutant *Irf8K79E* (Fig. 6g). Furthermore, transfer of WT *Irf8*, but not the mutant, restored the ability to increase LC3II protein expression after *Listeria* infection (Fig. 6h, left and middle panels). Consequently, *Irf8* gene transfer led to a marked increase in LC3-positive vesicles (Fig. 6h, right panel and Supplementary Fig. 7b). These data provide strong evidence that IRF8-dependent transcription plays a major role in autophagic control of *Listeria* infection in MΦs.

IRF8 regulates starvation and M-CSF-induced autophagy.

Starvation is one of the best-studied autophagy models¹. Because starvation is seemingly unrelated to innate immunity, and have not been studied extensively in MΦs, we asked whether starvation induces autophagy in MΦs and if so, whether IRF8 plays a role. We found that many autophagy genes were induced in WT MΦs on starvation, although the pattern of induction differed from that seen by IFNγ/TLR or *Listeria* infection (Fig. 7a). Notably, the genes active in early stages of autophagy were induced after starvation, whereas those involved in later stages were not. Moreover, *Irf8* itself was also induced after starvation in WT cells, although modestly. In contrast, these genes were not induced in *Irf8*^{-/-} MΦs at comparable levels. Basal expression of many autophagy genes was also lower in *Irf8*^{-/-} MΦs than WT cells. Interestingly, *Tfeb*, a master regulator of starvation-induced autophagy, involved in lysosomal biogenesis, was induced in MΦs in an IRF8-dependent manner¹⁶. On the other hand, *Foxo3*, the transcription factor that regulates autophagy in atrophying muscle cells was expressed at similar levels in WT and *Irf8*^{-/-} MΦs, and was not induced by any of the stimuli tested in this study (Supplementary Fig. 9)¹⁷.

Rescue experiments in Supplementary Fig. 10a showed that transfer of WT *Irf8*, but not *Irf8K79E* mutant into *Irf8*^{-/-} MΦs restored the expression of five autophagy genes during starvation condition. Thus, starvation activates transcription of multiple autophagy genes in MΦs in an IRF8-dependent manner. We next

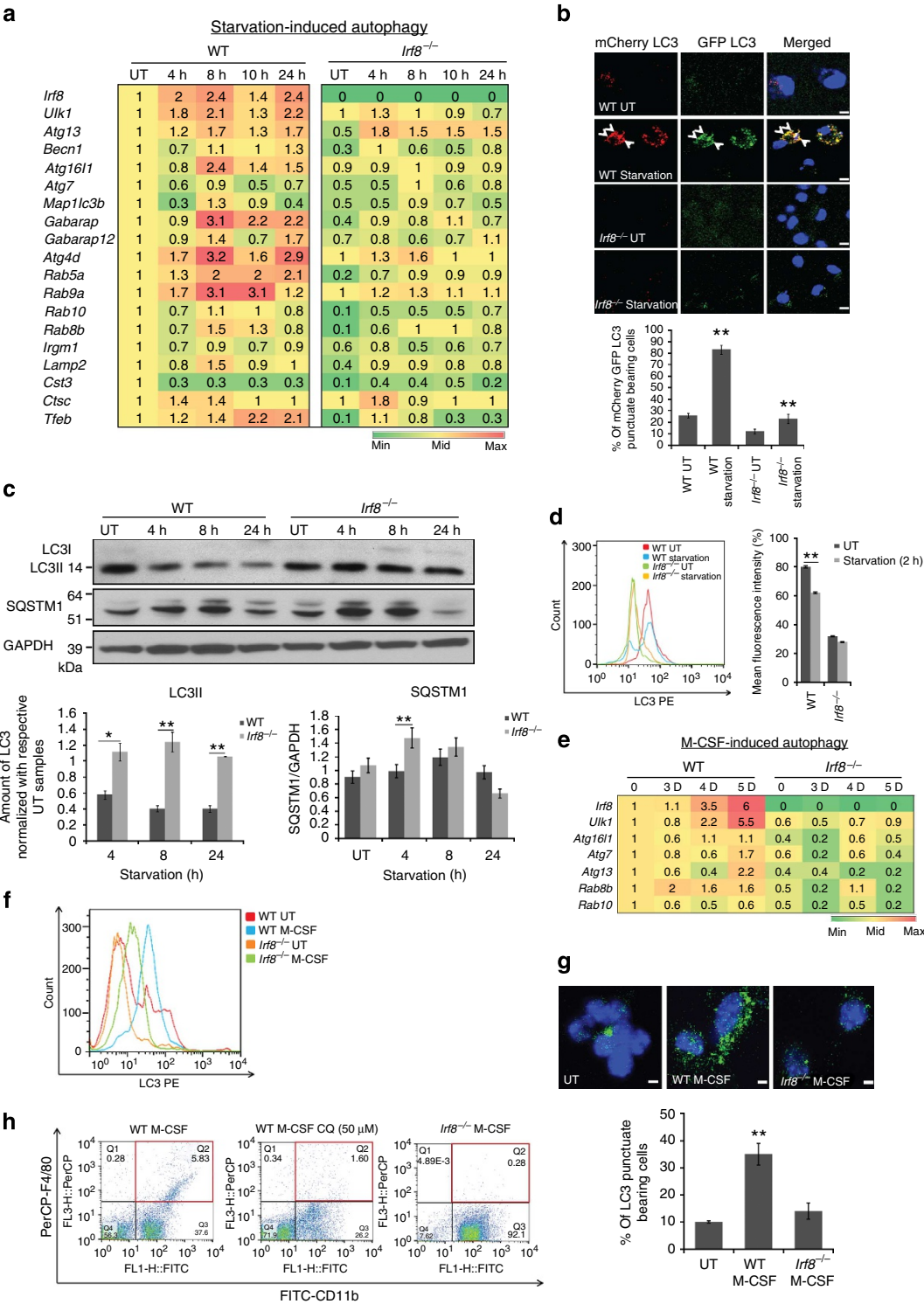
examined mCherry-EGFP-LC3 fluorescent signals after starvation and found many fluorescence-positive vesicles in WT MΦs, while only diffuse signals in *Irf8*^{-/-} MΦs, indicating that starvation induces autophagosome formation in WT MΦs, but this process is severely impaired in *Irf8*^{-/-} MΦs (Fig. 7b, see quantification below). LC3 flux analysis in Fig. 7c showed that the amount of LC3II fell 8 and 24 h after starvation in WT MΦs. Whereas, the amounts of LC3 remained similar in *Irf8*^{-/-} MΦs under these conditions, suggesting that LC3 was autophagically processed in WT MΦs as reported for other cells, and this process was defective in *Irf8*^{-/-} MΦs⁴⁴ (Fig. 7c top and bottom). Consistent with the immunoblot data, flow cytometry analysis in Fig. 7d found that amounts of membrane-bound LC3 were reduced after starvation in WT MΦs, but not in *Irf8*^{-/-} MΦs. Cell viability assay confirmed that the reduced LC3 amounts in WT MΦs during starvation were not due to toxicity of nutrient deprivation (Supplementary Fig. 10b). Above assays were performed in the absence of bafilomycin A1. To assess the role of IRF8 in autophagosome formation, we performed similar assays in the presence of bafilomycin A1. In immunoblot assays, amounts of LC3II appeared similar in WT MΦs and *Irf8*^{-/-} MΦs after starvation (Supplementary Fig. 10c). These data support lysosomal processing of LC3 in WT MΦs as suggested above. Nonetheless, the results differed from those seen by all other stresses tested, including M-CSF (below), in which LC3II levels were lower in *Irf8*^{-/-} MΦs than WT MΦs in the presence of bafilomycin A1. This difference may be due to differential influence of IRF8 on LC3II protein levels under different stresses. Importantly, however, EGFP-positive punctae as well as membrane-bound LC3 were markedly lower in *Irf8*^{-/-} MΦs relative to WT MΦs in the presence of bafilomycin A1 (see microscopy and flow cytometry data in Supplementary Fig. 10d,e). Overall, these results point to a deficiency in forming intact autophagosomes in *Irf8*^{-/-} MΦs in addition to defects in the subsequent steps such as lysosomal fusion and protein processing. Further, we found that the amounts of SQSTM1 were higher in *Irf8*^{-/-} MΦs than WT MΦs during 8 h of starvation both with or without bafilomycin A1 (Fig. 7c and Supplementary Fig. 10c). We also found that starvation downregulated phospho-mTOR in WT and *Irf8*^{-/-} MΦs (Supplementary Fig. 10f), as shown in other cell types¹ (Supplementary Fig. 4). Thus, *Irf8*^{-/-} MΦs, although capable of downregulating mTOR on starvation, are nevertheless defective in starvation-induced autophagy.

Recent reports document that autophagy promotes M-CSF-mediated monocyte to MΦ differentiation *in vitro*^{11,12}. In view of the fact that IRF8 drives MΦ differentiation, it was of interest to test whether IRF8 affects M-CSF-mediated autophagy during MΦ

Figure 6 | IRF8 is required for the autophagic clearance of *Listeria*. (a) WT and *Irf8*^{-/-} MΦs (10⁶) were infected with *Listeria* (5 × 10⁷) and bacterial transcripts were detected by qRT-PCR, normalized by *Gapdh*. Data represent the average of three independent experiments. *P* ≤ 0.05 (Student's *t*-test). (b) Autophagy gene expression in indicated MΦs was detected as above and normalized to those in uninfected WT MΦs. Data represent the average of three independent experiments. *P* ≤ 0.05 (Student's *t*-test). (c) Bacterial yields tested by the colony-forming unit (c.f.u.) assay. Some WT MΦs were treated with bafilomycin A1 (200 nM). Values represent the average of three determinations ± s.d. (d) Immunoblot analysis of LC3 and SQSTM1 in *Listeria*-infected WT and *Irf8*^{-/-} MΦs in the presence of bafilomycin A1 (200 nM). Below: amounts of LC3 and SQSTM1 from three independent samples were quantified by ImageJ software. ***P* ≤ 0.01 (Student's *t*-test). See Supplementary Fig. 7a for LC3 and SQSTM1 amounts in the absence of bafilomycin A1. (e) Distribution of *Listeria* antigens and LC3 after 36 h of *Listeria* infection in immunostaining. Arrow heads: LC3-associated *Listeria*. Scale bar, 20 μm. Below: the percentage of cells showing the co-localization of LC3 and *Listeria* antigens. Values represent the average of three independent experiments ± s.d. with ***P* ≤ 0.01 (Student's *t*-test). (f) Bacterial yields in MΦs infected with *Listeria* for 24 h and treated with Act D (2 μg ml⁻¹). Data represent the average of three determinations ± s.d. See Supplementary Fig. 8 for details of Act D effects. (g) *Irf8*^{-/-} MΦs transduced with *Irf8* vector were infected with *Listeria* for 36 h and autophagy gene expression was detected as above. The numbers represent transcript levels normalized by those with empty vector. *Irf8* transcripts were normalized by *gapdh*. Values are the average of three experiments. *P* ≤ 0.05 (Student's *t*-test). *Hprt*: a negative control. (h) Left and middle: *Irf8*^{-/-} MΦs transduced as above were tested for LC3II using GAPDH as a control. The amounts of LC3II in two independent experiments were quantified using ImageJ software. ***P* ≤ 0.01 (Student's *t*-test). Right: *Irf8*^{-/-} MΦs expressing mCherry-EGFP-LC3 were transduced as above and infected with *Listeria* for 36 h and fluorescent LC3 signals was visualized by confocal microscopy. See Supplementary Fig. 7b for microscopy image with controls.

maturation^{19,21}. qRT-PCR analysis in Fig. 7e showed that expression of various autophagy genes increased during 5 days of WT BM cell cultures with M-CSF. In contrast, none of these genes were induced in *Irf8*^{-/-} cells. *Irf8* was strongly induced in WT cells cultured in M-CSF³³. Flow cytometric analysis showed that membrane-bound LC3 signals increased in WT cell cultures, but only modestly in *Irf8*^{-/-} cell cultures (Fig. 7f and Supplementary Fig. 11a). LC3 signals in UT cells were also lower in *Irf8*^{-/-} cells than WT cells. Furthermore, immunostaining analysis in Fig. 7g showed that the number of

cells with LC3 vesicles was noticeably higher in WT cells than *Irf8*^{-/-} cells. In accordance, immunoblot analysis showed that the levels of LC3II increased in WT cells during M-CSF, but in *Irf8*^{-/-} cells LC3 levels only meagerly increased with or without bafilomycin A1, indicating defective autophagosome formation and fusion with lysosomes (Supplementary Fig. 11b). The amounts of SQSTM1 were higher in M-CSF treated *Irf8*^{-/-} cells as compared with WT cells also with and without bafilomycin A1, suggesting greater accumulation of SQSTM1 in *Irf8*^{-/-} cells than WT cells (Supplementary Fig. 11b).



As expected, WT cell cultures generated many more cells expressing authentic MΦ markers, F4/80 and CD11b, compared with *Irf8*^{-/-} cell cultures (Fig. 7h). Treatment with Chloroquine to inhibit autolysosome function led to a marked reduction in F4/80 and CD11b-positive cells (Fig. 7h). These results support a role for autophagy in M-CSF-mediated MΦ differentiation in which IRF8 plays an important part.

Discussion

In this study, we show that IRF8 stimulates a series of autophagy genes on various stresses known to activate autophagy in MΦs, including IFNγ/TLR, *Listeria* infection, starvation and M-CSF stimulation. Consequently, IRF8 was found to play a critical role in autophagic progression, from autophagosome formation to autolysosomes and degradation of cellular components. Moreover, on *Listeria* infection, IRF8 critically contributed to the elimination of the intracellular bacteria. It is clear that IRF8, although not an autophagy effector by itself, is indispensable for the execution of autophagy in MΦs. In most cases, autophagy

genes regulated by IRF8 ranged widely, covering essentially the entire autophagic pathways, from the initial autophagosome activation to the final lysosomal degradation of captured targets, indicating that IRF8 influences autophagic events from the beginning to the end. Because many of autophagy genes were transcriptionally activated on stress in MΦs, efficient autophagic execution in these cells must require transcriptional input. Our data show that IRF8 activates transcription of autophagy genes directly or in cooperation with other factors, since (a) IRF8 bound to the promoter of multiple autophagy genes and (b) expression of these and additional autophagy genes was rescued by *Irf8* gene transfer in *Irf8*^{-/-} MΦs. Consequently, *Irf8*^{-/-} MΦs were impaired in many autophagic functions, ranging from defective autophagosome formation to autophagic degradation of cellular components, including ubiquitin-bound proteins such as SQSTM1. Most importantly, *Irf8*^{-/-} MΦs were unable to control the growth of *Listeria*.

On the basis of the central role that IRF8 plays in all autophagy settings we tested, IRF8 may be regarded as one of the master

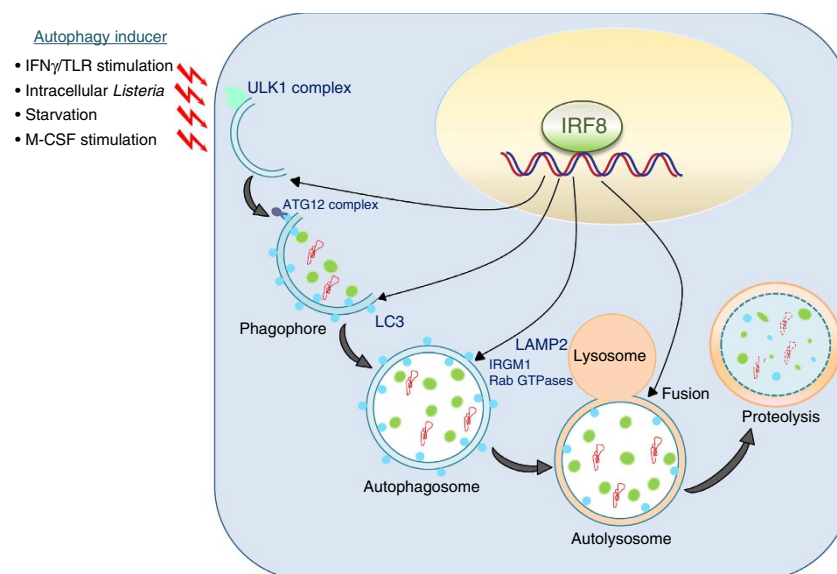


Figure 8 | A model for IRF8-dependent autophagy in MΦs. On various stresses (IFNγ/TLR stimulation, *Listeria* infection, starvation and M-CSF stimulation), IRF8 is activated and promotes the expression of a series of autophagy genes. These genes encode factors active at various stages of autophagy, largely covering the whole autophagic cascade. *Irf8*^{-/-} MΦs are defective in autophagic activation and fail to degrade target ubiquitin-conjugated factors, organelle and intracellular pathogens. Together, IRF8 acts as an autophagy master regulator in MΦs to coordinate stress responses critical for innate immunity.

Figure 7 | IRF8 stimulates starvation and M-CSF-induced autophagy. (a) Autophagy gene expression in WT and *Irf8*^{-/-} MΦs after starvation was detected by qRT-PCR and normalized by transcript values in UT WT cells. The number represents the average of three independent experiments. $P \leq 0.05$ (Student's *t*-test). (b) WT and *Irf8*^{-/-} MΦs expressing mCherry-EGFP-LC3 after starvation for 6 h and LC3 fluorescence signals (arrow heads) were visualized. Below: the percentage of cells with double-positive LC3 signals. Data represent the average of three independent experiments. $**P \leq 0.01$ (Student's *t*-test). Scale bar, 20 μm. See Supplementary Fig. 10d for LC3 fluorescence signals in the presence of bafilomycin A1. (c) Immunoblot detection of LC3II and SQSTM1 in starved WT and *Irf8*^{-/-} MΦs. Below: the amounts of total LC3 and SQSTM1 in three independent samples quantified by ImageJ software. $*P \leq 0.05$ and $**P \leq 0.01$ (Student's *t*-test). See Supplementary Fig. 10c for LC3 and SQSTM1 amounts in the presence of bafilomycin A1. (d) Left panel: membrane-bound LC3 in WT and *Irf8*^{-/-} MΦs after 2 h starvation was detected by flow cytometry. The histogram is a typical example of three independent experiments. Right panel: mean fluorescence intensity of membrane-bound LC3. Values represent the mean of three independent experiments. $**P \leq 0.01$ (Student's *t*-test). See Supplementary Fig. 10e for fluorescence-activated cell sorting detection in the presence of bafilomycin A1. (e) Autophagy gene expression in WT and *Irf8*^{-/-} BM cells cultured in M-CSF was detected by qRT-PCR, and transcripts were normalized by values in WT cells on day 0. The number represents the average of three independent experiments. $P \leq 0.05$ (Student's *t*-test). (f) Membrane-bound LC3 in WT and *Irf8*^{-/-} MΦs cultured in M-CSF for 4 days was detected by flow cytometry. The histogram is a typical example of three independent experiments. Similar results were observed with MΦs on days 3 and 5 (See Supplementary Fig. 11a). (g) LC3 vesicles in WT and *Irf8*^{-/-} MΦs cultured in M-CSF for 3 days was detected by immunostaining. Below: the percentage of cells bearing LC3 vesicles. $**P \leq 0.01$ (Student's *t*-test). Scale bar, 20 μm. (h) Expression of F4/80 and CD11b was detected in WT and *Irf8*^{-/-} MΦs cultured in M-CSF for 3 days by flow cytometry. Chloroquine (50 μM) was added in the middle panel for the final 18 h. Similar results were observed in three independent experiments.

regulators of M Φ autophagy. In many cases, autophagy is likely to be initiated by the preexisting cytoplasmic autophagy effectors. Nevertheless, some autophagy components are presumably turned over to be replaced by newly synthesized components. There are a few examples where proteins required for autophagy are synthesized during autophagic events by distinct transcription factors^{16,17}. For example, muscle atrophy-associated autophagy requires FOXO3, a transcription factor of the forkhead family¹⁷. FOXO3 is activated by starvation and it then induces a number of autophagy genes to stimulate lysosomal proteolysis, which leads to the degradation of cellular components and muscle cell atrophy. Second, TFEB, a transcription factor of the bHLH family, regulates genes important for biogenesis and functions of lysosomes. Through this action, TFEB coordinates autophagy-mediated lipid metabolism¹⁶. In these cases, FOXO3 and TFEB provide a mechanism to coordinate autophagic processes. The function of IRF8 in M Φ autophagy found in this study is comparable to those of FOXO3 and TFEB, although these factors act on different aspects of autophagy in different cell types. The above reports, combined with our results, lead us to a line of thinking that activities of individual autophagy genes are organized as a network by a central regulator that integrates separate autophagic events to achieve orderly elimination of target factors. FOXO3 and TFEB may thus represent the founding members of autophagy master regulators. It is not surprising that autophagy master regulators so far identified are transcription factors, given that they regulate multiple genes in a signal-dependent manner.

While IRF8 was important for the execution of autophagy after varying stresses, we noted that the patterns of autophagy gene induction varied under different stress conditions. For example, *Atg7*, downregulated by IFN γ /TLR and starvation was, however, upregulated by *Listeria* infection. In addition, the range of autophagy genes rescued by *Irf8* gene transfer varied among different stresses. Moreover, IRF8 influenced LC3II levels in starvation differently from other stresses.

Autophagic competence is a vital requirement for the function and survival of M Φ s and DCs, since these cells, acting as sentinels, must detect and eliminate invading pathogens rapidly. M Φ s and DCs thus produce a large amount of reactive oxygen species and nitric oxide as part of the antimicrobial defense. These compounds, however, as free radicals, likely damage the integrity of cellular components, which need to be processed in a timely manner. IRF8 was induced by classic stresses, IFN γ /TLR, starvation and *Listeria* infection. Although not regarded as a classic stress factor, M-CSF too may involve some types of stress, given that it activates the stress kinase JNK¹². Thus, one could envisage that IRF8 may be adopted by M Φ s and DCs to meet heightened requirement for responding to stresses by augmenting autophagic functions.

It was striking that *Listeria* infection caused a dramatic and prolonged expression of many autophagy genes along with that of *Irf8* itself. The high, sustained expression of autophagy genes indicate that many autophagy factors were newly synthesized and replenished in M Φ s during infection in an IRF8-dependent manner to support autophagic control of bacterial growth. Our observation that a brief Act D treatment gave way to rapid bacterial growth in WT M Φ s may further support the view that continuous autophagy gene transcription is required for sustained resistance to *Listeria* infection. Furthermore, our results that LC3 co-localized with *Listeria* antigens are consistent with the report that autophagy plays a critical role in combating *Listeria* infection by linking ubiquitin pathways⁴⁵. Moreover, our observations that *Irf8* gene transfer led to a partial rescue of autophagosome formation provide compelling evidence that IRF8-dependent

transcription critically contributes to the control of *Listeria* infection in M Φ s.

It is noteworthy that IRF8 has been known to play a crucial role in combating *Listeria* infection since 1997 (ref. 23). Our results are consistent with this early study and provide deeper insight into the mechanism by which IRF8 confers resistance to the bacteria. In a similar context, it has been shown that IRF8 is essential for controlling infection by other bacteria, including *M. tuberculosis*: mutations in *Irf8* are associated with increased susceptibility to *Mycobacteria* infection in mice and humans^{24–26}. However, underlying molecular mechanisms have not been fully clarified. In light of recent reports that autophagic clearance is critically required for controlling *Mycobacteria* infection, it seems likely that autophagy is an important means by which IRF8 exerts antimycobacterium activity^{6,7}. IRF8 may also augment other aspects of innate immunity through autophagy, such as major histocompatibility complex II-mediated antigen presentation to TLR-dependent type I IFN induction^{4,9}.

In conclusion, IRF8 activates autophagic cascades in M Φ s at the level of transcription, and orchestrates capturing and elimination of endogenous targets and infectious pathogens.

Methods

Mice and cells. WT and *Irf8*^{−/−} mice on C57BL/6 background¹⁸ were maintained in the NICHD animal facility. All animal work conformed to the NICHD animal care and use committee guidelines. BM mononuclear cells isolated from age-matched mice (female, 6–10 weeks old) were cultured as described previously²⁰. In brief, BM mononuclear cells were cultured in complete RPMI medium (RPMI, 10% fetal bovine serum, 1 mM sodium pyruvate, 0.1 mM NEAA, 0.05 mM β -mercaptoethanol, 2 mM L-glutamine, 100 U ml^{−1} streptomycin/penicillin) in the presence of Flt3L (100 ng ml^{−1}) or M-CSF (20 ng ml^{−1}) for 5 to 6 days to generate DCs and M Φ s, respectively. DCs were stimulated with 100 ng ml^{−1} of LPS (Sigma) and 1 μ g ml^{−1} of CpG 1826 (Lofstrand Labs) for 4–6 h for microarray analysis. M Φ s were treated with IFN γ (100 U ml^{−1}) overnight followed by stimulation with LPS (100 ng ml^{−1}) and CpG 1826 (1 μ g ml^{−1}) for indicated periods. For starvation, M Φ s were washed with PBS and incubated in Earle's balanced salt solution at 37 °C for indicated times. In some cases, M Φ s were treated with Act D (Sigma, cat. no. A1410) at 2 μ g ml^{−1} for indicated times. For bacterial infection, M Φ s were stimulated with IFN γ (100 U ml^{−1}) in antibiotics free media for 20 h followed by infection with *Listeria monocytogenes* 10403S at a bacteria to cell ratio of 50:1 and maintained in complete media for indicated times⁴⁶. Bacterial yields were measured by colony-forming unit assay after plating serially diluted culture supernatants of infected cells on BHI agar (Sigma, cat. no. 70138). For M-CSF treatment, BM-derived mononuclear cells were incubated in media containing M Φ -colony-stimulating factor (M-CSF (Peprotech), 20 ng ml^{−1}) at 37 °C for indicated days.

Microarray analysis. Total RNA from unstimulated and TLR-stimulated DCs was processed through RNeasy column (Qiagen) to remove possible DNA contaminants. Two independent RNA samples prepared from UT and TLR-stimulated DCs of WT and *Irf8*^{−/−} mice were subjected to microarray analysis using the Affymetrix Genechip Mouse 430 A 2.0 through Cogenics Inc. In brief, 1 μ g of total RNA was converted to double-stranded complementary DNA with the Bioarray Single-Round RNA Amplification and Labeling Kit (Enzo Life Sciences) and multiple copies of biotinylated cRNA were synthesized by *in vitro* transcription with the Bioarray HighYield RNA Transcript Labeling Kit (Enzo Life Sciences), and assessed for quality by an Agilent Bioanalyzer. Six and a half μ g of biotinylated cRNA spiked with bioB, bioC, bioD was hybridized to the array for 16 h at 45 °C. Arrays were washed, stained in an Affymetrix GeneChip Fluidics Station and scanned with an Affymetrix GeneChip Scanner 3000. Quality checks and data analyses were carried out using Affymetrix GeneChip Operating Software (GCOS) and Expression Console. All arrays have passed Cogenics' internal QC metrics. Values with $P \leq 0.05$ and two-fold cutoff were considered significant. Analysis of variance (including *t*-tests), was used to identify differentially expressed genes²⁸. Raw data files have been deposited in the NCBI Gene Expression Omnibus under the accession number GSE64666. A complete list of IRF8 depended differentially expressed genes is provided in Supplementary Table 2.

GO analyses were performed using Database for Annotation, Visualization and Integrated Discovery (DAVID; <http://david.abcc.ncifcrf.gov/>)⁴⁷.

Immunofluorescence staining and flow cytometry analysis. M Φ s grown on coverslips were stimulated with required treatment as above. Some cells were treated with 200 nM bafilomycin A1 (Invivogen, cat. no. tlr1-baf) for 2 h, fixed with 4% paraformaldehyde, permeabilized with 0.1% Triton-X-100 for 5 min and

blocked by 5% bovine serum albumin with 0.1% Tween 20. Cells were incubated for 5 h with antibody against LC3 (MBL, cat. no. M152-3) or LAMP2 (ProSci, cat. no. 3627), SQSTM1 (MBL, cat. no. PM045), Ubiquitin (Santacruz, cat. no. sc8017) or *Listeria* (Abcam, cat. no. ab35132) diluted at 1:1,000 followed by 1 h incubation with goat Alexa-488/Alexa-592 anti-rabbit or anti-mouse antibody (Molecular Probes). Cells were counterstained with DAPI for DNA. To detect autophagic vacuoles, mitochondria and lysosomes, cells were incubated with 10 μ M Monodansylcadaverine (Sigma 30432), 50 nM MitoTracker red (MT, Invitrogen M22426) or 50 nM LysoTracker-Red (Invitrogen L7528). Stained cells were viewed on a confocal microscope (Leica, SP2) with a $\times 63$ oil immersion objective. Membrane-bound LC3 was detected by the flow cytometry method as described³⁷. In brief, the cells were washed with PBS containing 0.05% saponin and incubated with mouse anti-LC3 and then with PE-conjugated goat anti-mouse antibody (Biolegend, cat. no. 405307). Data were analysed using the FlowJo software.

Electron microscopy. MΦs were fixed in 0.1-M sodium cacodylate buffer pH 7.3 containing 2% paraformaldehyde, 2.5% glutaraldehyde (EMS, 15949) and post fixed with 2% osmium tetroxide in 0.1-M sodium cacodylate buffer and processed as described³⁵. Samples were sectioned on a Leica Ultracut UC6 ultramicrotome. Thin sections (70 nm) were post stained with 3% uranyl acetate and Reynolds lead citrate and examined on FEI Tecnai Spirit G2 TEM. Digital images were captured on an FEI Eagle camera. Samples were processed for TEM by the Cell Imaging Facility at Northwestern University Feinberg School of Medicine.

Retroviral transduction. The assay was performed as described^{18,20,29}. Relevant details are provided in the figure legends. For retroviral transduction, HEK293T retroviral packaging cells were transiently transfected with pMSCV retroviral vectors with WT *Irf8* or *Irf8K79E* using Lipofectamine 2000 according to the manufacturer's protocol. Retroviral supernatants were collected at 48 h. MΦs were transduced by spinoculation (3,000 r.p.m., 33 °C, 1 h) with the retroviral supernatant supplemented with 4 μ g ml⁻¹ polybrene. Transduced cells were selected with 2 μ g ml⁻¹ puromycin 48 h post spinoculation.

Quantitative RT-PCR. The assay was performed as described^{18,20,29}. In brief, total RNA was extracted using Trizol (Invitrogen). Complementary DNA was prepared from 1 μ g of RNA with Superscript II RT (Invitrogen) and random hexamer primers (Promega). PCR was carried out by ABI 7500 (Applied Biosystems) using a standard protocol for appropriate cycles. Primers used for PCR are listed in Supplementary Table 3. Transcript levels were normalized by glyceraldehyde-3-phosphate dehydrogenase (*Gapdh*) and fold changes were calculated by the C_t method.

Immunoblot assay. Cell lysates and prestained molecular weight markers were subjected to SDS-polyacrylamide gel electrophoresis and transferred to a nitrocellulose membrane. The membranes were blocked with 5% non-fat milk in TBST (Triton-X-100 containing Tris-buffered saline), incubated with various antibodies (1:3,000) for 1–2 h, washed with TBST, and stained with anti-rabbit or anti-mouse IgG conjugated to peroxidase (1:5,000). Immunoreactivity was visualized by enhanced chemiluminescence (ECL kit, Thermo Fisher Scientific). Full immunoblots with indicated areas of selection are provided in Supplementary Fig. 12.

Chromatin immunoprecipitation assay. ChIP assays were performed as previously described^{18,20,29}. In brief, 2.5–10 $\times 10^6$ MΦs were crosslinked with 0.75% formaldehyde and quenched in 0.125 M glycine. Cell lysates were sonicated and immunoprecipitated with 0.5 μ g of rabbit IgG antibody (Sigma) or anti-IRF8 antibody (affinity purified)²⁰. The immunoprecipitated DNA was eluted and amplified by real-time PCR using an ABI 7500 (Applied Biosystems). Values were normalized to corresponding input control and expressed as fold enrichment. Primers used for PCR are listed in Supplementary Table 3.

Statistical analysis. Student's *t*-test was used as statistical analysis by using Microsoft Excel.

References

- He, C. & Klionsky, D. J. Regulation mechanisms and signaling pathways of autophagy. *Annu. Rev. Genet.* **43**, 67–93 (2009).
- Mizushima, N., Yoshimori, T. & Ohsumi, Y. The role of Atg proteins in autophagosome formation. *Annu. Rev. Cell Dev. Biol.* **27**, 107–132 (2011).
- Delgado, M. A. & Deretic, V. Toll-like receptors in control of immunological autophagy. *Cell Death Differ.* **16**, 976–983 (2009).
- Levine, B., Mizushima, N. & Virgin, H. W. Autophagy in immunity and inflammation. *Nature* **469**, 323–335 (2011).
- Matsuzawa, T. *et al.* IFN- γ elicits macrophage autophagy via the p38 MAPK signaling pathway. *J. Immunol.* **189**, 813–818 (2012).
- Bradford, S. B. *et al.* Autophagy as an immune effector against tuberculosis. *Curr. Opin. Microbiol.* **16**, 355–365 (2013).
- Castillo, E. F. *et al.* Autophagy protects against active tuberculosis by suppressing bacterial burden and inflammation. *Proc. Natl Acad. Sci. USA* **109**, 3168–3176 (2012).
- Henault, J. *et al.* Noncanonical autophagy is required for type I interferon secretion in response to DNA-immune complexes. *Immunity* **37**, 986–997 (2012).
- Lee, H. K. *et al.* *In vivo* requirement for Atg5 in antigen presentation by dendritic cells. *Immunity* **32**, 227–239 (2010).
- Mostowy, S. *et al.* p62 and NDP52 proteins target intracytosolic *Shigella* and *Listeria* to different autophagy pathways. *J. Biol. Chem.* **286**, 26987–26995 (2011).
- Jacquel, A. *et al.* Autophagy is required for CSF-1-induced macrophagic differentiation and acquisition of phagocytic functions. *Blood* **119**, 4527–4531 (2012).
- Zhang, Y., Morgan, M. J., Chen, K., Choksi, S. & Liu, Z. G. Induction of autophagy is essential for monocyte-macrophage differentiation. *Blood* **119**, 2895–2905 (2012).
- Itakura, E. & Mizushima, N. p62 Targeting to the autophagosome formation site requires self-oligomerization but not LC3 binding. *J. Cell Biol.* **192**, 17–27 (2011).
- Komatsu, M. *et al.* Homeostatic levels of p62 control cytoplasmic inclusion body formation in autophagy-deficient mice. *Cell* **131**, 1149–1163 (2007).
- MacMicking, J. D. Interferon-inducible effector mechanisms in cell-autonomous immunity. *Nat. Rev. Immunol.* **12**, 367–382 (2012).
- Settembre, C. *et al.* TFEB controls cellular lipid metabolism through a starvation-induced autoregulatory loop. *Nat. Cell Biol.* **15**, 647–658 (2013).
- Zhao, J. *et al.* FoxO3 coordinately activates protein degradation by the autophagic/lysosomal and proteasomal pathways in atrophying muscle cells. *Cell Metab.* **6**, 472–483 (2007).
- Tamura, T. *et al.* IFN regulatory factor-4 and -8 govern dendritic cell subset development and their functional diversity. *J. Immunol.* **174**, 2573–2581 (2005).
- Tamura, T., Yanai, H., Savitsky, D. & Taniguchi, T. The IRF family transcription factors in immunity and oncogenesis. *Annu. Rev. Immunol.* **26**, 535–584 (2008).
- Chang, T. H., Xu, S., Tailor, P., Kanno, T. & Ozato, K. The small ubiquitin-like modifier-deconjugating enzyme sentrin-specific peptidase 1 switches IFN regulatory factor 8 from a repressor to an activator during macrophage activation. *J. Immunol.* **189**, 3548–3556 (2012).
- Kurotaki, D. *et al.* Essential role of the IRF8-KLF4 transcription factor cascade in murine monocyte differentiation. *Blood* **121**, 1839–1849 (2013).
- Alter-Koltunoff, M. *et al.* Innate immunity to intraphagosomal pathogens is mediated by interferon regulatory factor 8 (IRF-8) that stimulates the expression of macrophage-specific Nramp1 through antagonizing repression by c-Myc. *J. Biol. Chem.* **283**, 2724–2733 (2008).
- Fehr, T. *et al.* Crucial role of interferon consensus sequence binding protein, but neither of interferon regulatory factor 1 nor of nitric oxide synthesis for protection against murine listeriosis. *J. Exp. Med.* **185**, 921–931 (1997).
- Hambleton, S. *et al.* IRF8 mutations and human dendritic-cell immunodeficiency. *N. Engl. J. Med.* **365**, 127–138 (2011).
- Turcotte, K. *et al.* Icsbp1/IRF-8 is required for innate and adaptive immune responses against intracellular pathogens. *J. Immunol.* **179**, 2467–2476 (2007).
- Rocca, A. *et al.* Interferon regulatory factor 8-deficiency determines massive neutrophil recruitment but T cell defect in fast growing granulomas during tuberculosis. *PLoS ONE* **8**, e62751 (2013).
- Marquis, J. F. *et al.* Interferon regulatory factor 8 regulates pathways for antigen presentation in myeloid cells and during tuberculosis. *PLoS Genet.* **7**, e1002097 (2011).
- Shin, D. M., Lee, C. H. & Morse, 3rd H. C. IRF8 governs expression of genes involved in innate and adaptive immunity in human and mouse germinal center B cells. *PLoS ONE* **6**, e27384 (2011).
- Taylor, P., Tamura, T., Morse, 3rd H. C. & Ozato, K. The BXH2 mutation in IRF8 differentially impairs dendritic cell subset development in the mouse. *Blood* **111**, 1942–1945 (2008).
- Rusinova, I. *et al.* INTERFEROME v2.0: an updated database of annotated interferon-regulated genes. *Nucleic Acids Res.* **41**, D1040–D1046 (2013).
- Fujiwara, E., Washi, Y. & Matsuzawa, T. Observation of autophagosome maturation in the interferon- γ -primed and lipopolysaccharide-activated macrophages using a tandem fluorescently tagged LC3. *J. Immunol. Methods* **394**, 100–106 (2013).
- Qiao, Y. *et al.* Synergistic activation of inflammatory cytokine genes by interferon- γ -induced chromatin remodeling and Toll-like receptor signaling. *Immunity* **39**, 454–469 (2013).
- Tamura, T., Thotakura, P., Tanaka, T. S., Ko, M. S. & Ozato, K. Identification of target genes and a unique *cis* element regulated by IRF-8 in developing macrophages. *Blood* **106**, 1938–1947 (2005).
- Katayama, H., Yamamoto, A., Mizushima, N., Yoshimori, T. & Miyawaki, A. GFP-like proteins stably accumulate in lysosomes. *Cell Struct. Funct.* **33**, 1–12 (2008).

35. Goussetis, D. J. *et al.* Autophagic degradation of the BCR-ABL oncoprotein and generation of antileukemic responses by arsenic trioxide. *Blood* **120**, 3555–3562 (2012).
36. Klionsky, D. J. *et al.* Guidelines for the use and interpretation of assays for monitoring autophagy. *Autophagy* **8**, 445–544 (2012).
37. Eng, K. E., Panas, M. D., Karlsson Hedestam, G. B. & McInerney, G. M. A novel quantitative flow cytometry-based assay for autophagy. *Autophagy* **6**, 634–641 (2010).
38. Tanaka, Y. *et al.* Accumulation of autophagic vacuoles and cardiomyopathy in LAMP-2-deficient mice. *Nature* **406**, 902–906 (2000).
39. Kim, J. Y., Anderson, E. D., Huynh, W., Dey, A. & Ozato, K. Proteomic survey of ubiquitin-linked nuclear proteins in interferon-stimulated macrophages. *J. Interferon Cytokine Res.* **31**, 619–628 (2011).
40. Kim, J. Y. & Ozato, K. The sequestosome 1/p62 attenuates cytokine gene expression in activated macrophages by inhibiting IFN regulatory factor 8 and TNF receptor-associated factor 6/NF- κ B activity. *J. Immunol.* **182**, 2131–2140 (2009).
41. Yoshikawa, Y. *et al.* *Listeria monocytogenes* ActA-mediated escape from autophagic recognition. *Nat. Cell Biol.* **11**, 1233–1240 (2009).
42. Hamon, M., Bierne, H. & Cossart, P. *Listeria monocytogenes*: a multifaceted model. *Nat. Rev. Microbiol.* **4**, 423–434 (2006).
43. Travassos, L. H. *et al.* Nod1 and Nod2 direct autophagy by recruiting ATG16L1 to the plasma membrane at the site of bacterial entry. *Nat. Immunol.* **11**, 55–62 (2010).
44. Shvets, E., Fass, E. & Elazar, Z. Utilizing flow cytometry to monitor autophagy in living mammalian cells. *Autophagy* **4**, 621–628 (2008).
45. Ogawa, M. *et al.* Autophagy targeting of *Listeria monocytogenes* and the bacterial countermeasure. *Autophagy* **7**, 310–314 (2011).
46. Ohya, S., Xiong, H., Tanabe, Y., Arakawa, M. & Mitsuyama, M. Killing mechanism of *Listeria monocytogenes* in activated macrophages as determined by an improved assay system. *J. Med. Microbiol.* **47**, 211–215 (1998).
47. Huang da, W., Sherman, B. T. & Lempicki, R. A. Systematic and integrative analysis of large gene lists using DAVID bioinformatics resources. *Nat. Protoc.* **4**, 44–57 (2009).

Acknowledgements

We thank K.-T. Jeang, H.-S. Wang, S. Bradfute, V. Nagarajan, K.-A. McDonough and H. Yoshii for advice and critical reading of the manuscript. This work was supported by the Intramural Program of NICHD and NIAID, National Institutes of Health and NIH grants CA77816 and CA121192.

Author contributions

D.-M.S. and L.R. performed genome-wide expression analysis; D.J.G. and L.C.P. performed the electron microscopy of MΦs with autophagic activity; H.X. advised and participated in the *Listeria* infection studies; H.C.M. gave conceptual and practical advice throughout the study; M.G. and K.O. designed and performed the experiments, analysed the data and wrote the draft; K.O. steered the project and finalized the manuscript. All authors read and approved the submitted manuscript.

Additional information

Supplementary Information accompanies this paper at <http://www.nature.com/naturecommunications>

Competing financial interests: The authors declare no competing financial interests.

Reprints and permission information is available online at <http://npg.nature.com/reprintsandpermissions/>

How to cite this article: Gupta, M. *et al.* IRF8 directs stress-induced autophagy in macrophages and promotes clearance of *Listeria monocytogenes*. *Nat. Commun.* **6**:6379 doi: 10.1038/ncomms7379 (2015).